The Lipid Dependence of Melittin Action Investigated by Dual-Color Fluorescence Burst Analysis

Geert van den Bogaart,* Jacek T. Mika,* Victor Krasnikov,† and Bert Poolman*
*Biochemistry Department, and †Ultrafast Laser and Spectroscopy Laboratory, Groningen Biomolecular Science and Biotechnology Institute & Zernike Institute for Advanced Materials, University of Groningen, Groningen, The Netherlands

ABSTRACT Dual-color fluorescence-burst analysis was used to study melittin-induced leakage of macromolecules from liposomes of various lipid compositions. To perform dual-color fluorescence-burst analysis, fluorescently labeled size-marker molecules were encapsulated into liposomes, labeled with a second lipid-attached fluorophore. By correlating the fluorescence bursts, resulting from the liposomes diffusing through the detection volume of a dual-color confocal microscope, the distribution of size-marker molecules over the liposomes was determined. It was found that melittin causes leakage via two different mechanisms: 1), For liposomes composed of neutral bilayer-forming lipids, low melittin concentrations induced pore formation with the pore size depending on the melittin concentration. 2), For liposomes containing anionic and/or nonbilayer forming lipids, melittin induced fusion or aggregation of liposomes accompanied by a-specific leakage. Experiments with liposomes prepared from *Escherichia coli* lipid extracts and intact cells of *Lactococcus lactis* indicate that both mechanisms are physiologically relevant.

INTRODUCTION

Antimicrobial peptides are typically 12–50 amino acids long and play an important role in the innate immune response of the host organism. Over 800 antimicrobial peptides have been identified in species as diverse as bacteria, fungi, plants, and mammals (1) and they are a possible source of antibiotics for the pharmaceutical industry (2,3). The antimicrobial peptide melittin is a membrane disrupting agent, frequently used as a model for hemolytic activity (4) and is one of the best studied antimicrobial peptides to date (see Raghuraman and Chattopadhyay (5) for recent review). The strongly cationic (6+) melittin is the major component of the European honeybee (*Apis mellifera*) venom (6) and consists of 26 residues. In aqueous solution, melittin exists as either a monomer, with no defined secondary structure (7,8), or as a tetramer of α-helical peptides, depending on the concentration, ionic strength, and pH of the solution (8–10). It retains the amphiphilic α-helical structure in the membrane (11–13). Melittin has strong hemolytic and antimicrobial activity. It kills the cell by autoinsertion in the membrane, thereby forming large a-specific pores in both eukaryotic and prokaryotic membranes, leading to the leakage of cell content (14). Other cytotoxic mechanisms of action have also been proposed for melittin, including phospholipase D activation that leads to hydrolysis of phospholipids and probably activation of unknown transduction cascades (1,5,14–18).

It has been proposed that melittin induces pore formation via the toroidal mechanism (19,20), whereby the lipids, in particular the headgroups, together with the peptides line the pore. However, the toroidal mechanism is not undisputed and evidence is also available in favor of a barrel-stave arrangement of the melittin peptides in the pore (13,21–24). In the barrel-stave arrangement, the amphiphilic α-helical peptides insert in the membrane bilayer in such a way that the hydrophilic regions, but not the lipid headgroups, form the interior of the pore. There are also reports that claim that melittin disrupts membranes via the carpet-like mechanism (4,22). In the carpet-like mechanism, the peptides disrupt the membrane by forming an extensive layer of membrane-associated peptides and dissolve the membrane in a detergent-like manner with the helices orienting parallel to the surface. According to the widely accepted toroidal pore model, the pores consist of approximately four to eight melittin molecules (25,26). Regardless of the lipid composition, at low peptide/lipid ratios, the helical segments bind parallel to the membrane plane (27–31), at the depth of the glycerol groups (32). Each peptide would occupy an area of $\sim$6 nm^2 of membrane surface (33). Depending on the membrane composition, an increase in melittin concentration is thought to result in reorientation of melittin and insertion of the peptide perpendicular to the membrane plane (20), which induces the formation of pores (4,13,34).

The size of the melittin pore has been estimated to be between 3.5 and 4.5 nm in transmission electron microscopy (35) and 4.4 nm in neutron diffraction studies (20). This is in reasonable agreement with estimates from leakage experiments of macromolecules (25,34–41), where pore sizes ranging from 1.5 to 4.8 nm have been estimated. It should be noted, however, that the difference between the smallest (1.5 nm) and the largest pore-size estimate (4.8 nm) corresponds to molecules diffusing through the pore of $<$10 kDa up to $>$100 kDa and this apparent discrepancy might be of crucial importance for the mechanism of cell killing by melittin. It seems likely that these differences in pore-size estimates arise from differences in salt concentration, osmotic gradient, and lipid composition (1,5,42,43). For a better understanding

Submitted February 5, 2007, and accepted for publication March 7, 2007.

Address reprint requests to Bert Poolman, Tel.: 31-50-363-4190; Fax: 31-50-363-4165; E-mail: b.poolman@rug.nl.

Editor: Antoinette Killian.

0006-3495/07/07/154/10 $2.00

doi: 10.1529/biophysj.107.106005

of the action mechanism and the cytotoxic activity of melittin, a better knowledge of the pore formation and pore size is essential. Whether and how the pore size increases with increasing melittin concentration is still a matter of debate (20). In previous studies, phospholipid vesicles and erythrocyte membranes were used to monitor the leakage of macromolecules as a function of the melittin concentration, but the mechanism of pore formation and size could not be specified unambiguously (34–36,44).

We used dual-color fluorescence-burst analysis ((DCFBA); (45)) to probe the formation and size of the melittin pore. DCFBA allows one to determine the population distribution of size-marker molecules over the liposomes, thereby providing detailed information of the leakage process that is not readily obtained by conventional methods. Moreover, only small quantities of lipids are needed ($\sim\mu$g) and the data acquisition is relatively fast ($\sim$10 min), which allows for medium throughput screening of lipid compositions and melittin concentrations.

METHODS

Melittin and lipids

Melittin was obtained from GenScript (purity >95%; Piscataway, NJ). *Escherichia coli* total lipid extract, cholesterol, and the synthetic lipids 1,2-dioleoyl-*sn*-glycero-3-phosphocholine (DOPC), 1,2-dioleoyl-*sn*-glycero-3-phosphoethanolamine (DOPE), and 1,2-dioleoyl-*sn*-glycero-3-phosphatidylglycerol (DOPG) were from Avanti Polar Lipids (Alabaster, AL). Stock solutions of the lipids of 20 mg ml^{-1} in chloroform were prepared. The membrane dyes DiO (3,3′-dioctadecyloxacarbocyanine percholate; excitation wavelength $\lambda_{Ex} = 484$ nm, emission wavelength $\lambda_{Em} = 501$ nm) and DiD (1,1′-dioctadecyl-3,3,3′,3′-tetramethylindodicarbocyanine percholate; $\lambda_{Ex} = 644$ nm, $\lambda_{Em} = 665$ nm, Invitrogen, Carlsbad, CA) were added to the lipid stock solutions to ensure coincorporation in the vesicle membrane. For DOPC, a 1:4000 DiO (or DiD)/lipid ratio was used; for all other lipid mixtures, a 1:40,000 ratio was used. To obtain similar fluorescence-burst intensities, the probe/lipid ratio had to be 10-fold higher for DOPC. This is probably due to different interactions of DiO with zwitterionic DOPC when compared to the anionic DOPG. Experiments with liposomes composed of pure DOPG or a 1:1 mixture of DOPC/DOPG indicated that a 10-fold higher DiO concentration did not influence the leakage and fusion events (not shown).

Labeling of size-marker molecules and preparation of liposomes

Dextran molecules conjugated to Alexa fluor 647 (for the 10 kDa dextran, $\lambda_{Ex} = 650$ nm, $\lambda_{Em} = 668$ nm) and Oregon green 488 (for the 70 kDa dextran, $\lambda_{Ex} = 496$ nm, $\lambda_{Em} = 521$ nm) were from Invitrogen and dissolved in 50 mM potassium phosphate, pH 7.0, to a final concentration of 100 μM. The effective Stokes radii of the 10 and 70 kDa dextrans are 2.4 and 5.0 nm, respectively (36,46), although in solution they form ellipsoids with shortest radii of $\sim$2.0 nm (47). Glutathione, bovine pancreatic trypsin inhibitor (BPTI), and bovine α-lactalbumin were from Sigma-Aldrich (St. Louis, MO). Solutions of 100 μM BPTI and α-lactalbumin in 30 mM K-Hepes, pH 8.6, were labeled with 44 μM Alexa fluor 633 C5-maleimide (Invitrogen, $\lambda_{Ex} = 622$ nm, $\lambda_{Em} = 640$ nm, Mw = 1089 (45)) by incubating for 30 min at room temperature. The labeled macromolecules were separated from the unbound fluorophore by size exclusion chromatography (Nap10 columns, Amersham Biosciences, Piscataway, NJ) with subsequent buffer exchange to 50 mM potassium phosphate, pH 7.0. Glutathione was labeled with the same fluorophore in 50 mM potassium, pH 7.0. The purity of the proteins and efficiency of labeling was checked by SDS-PAGE and in-gel fluorescence.

For the liposome preparation, 250 μl (5 mg) of the lipid chloroform stock was dried by rotary evaporation at 50°C for 2 h. The lipid film was resuspended in 1 ml of 50 mM potassium phosphate, pH 7.0, with the size-marker molecules present at concentrations between 1 and 20 μM. After 3 times fast freezing (liquid nitrogen) and slow thawing (room temperature) and subsequent extrusion through 200 nm polycarbonate membranes (Avestin, Ottawa, Canada), the nonencapsulated size-marker molecules were separated from the liposomes by centrifugation (20 min, 270,000 $\times$ g, 4°C). For the DCFBA measurements, the liposomes were resuspended in 50 mM potassium phosphate, pH 7.0, to a final concentration of 80 μg of lipid ml^{-1}.

DCFBA measurements

DCFBA measurements were performed as described previously (45). Briefly, the fluorescently labeled size-marker molecules were encapsulated in liposomes that were labeled with a second fluorophore (the lipid analog DiO or DiD). The fluorescent bursts, resulting from the diffusion of the liposomes through the detection volume of a dual-color confocal microscope (45), were recorded for at least 10 min (Fig. 1). During this period, >1000 liposomes passed through the focal volume (Fig. 2). For all the fluorescent bursts above a certain offset, the integrated intensities of both the fluorescent lipid analog and the size-marker molecules were calculated. The size-marker concentration (C) of the i^{th} liposome (burst) could then be obtained by division:

$$C_i = \frac{\int_{t_1}^{t_2} I_{SM} dt}{\left(\int_{t_1}^{t_2} I_L dt\right)^{\frac{3}{2}}}, \quad (1)$$

where the fluorescence of the lipid marker (I_L) is above a certain offset between t_2 and t_1 and I_{SM} is the fluorescence of the size marker. In Eq. 1, the signals are normalized because the lipid analog is associated with the surface of the liposomes and the size-marker is present in the vesicles. As a function of liposome radius, I_{SM} and I_L thus scale to the power of 3 and 2, respectively (45). From C_i, the average concentration C_{av} over all the liposomes could be calculated:

$$C_{av} = \frac{1}{N}\sum_{i=1}^{N} C_i, \quad (2)$$

where N corresponds to the number of liposomes (45).

RESULTS

Pore formation

The effect of the lipid composition on the melittin pore size was studied using DCFBA, which enables rapid measurements of leakage with single liposome resolution (45). The liposomes were labeled with the fluorescent lipid analog DiO or DiD and encapsulated with size-marker molecules that were labeled with a second fluorophore. Because both the fluorescent lipid analog and the size-marker molecules are liposome associated, both fluorescence signals coincide (Fig. 1, *top panel*). Upon pore formation, the size-marker molecules with dimensions smaller than the diameter of the melittin pores leak out (Fig. 1, *bottom panel*). This results in the loss of coincidence of the signals. In Fig. 2 *A*, part of a

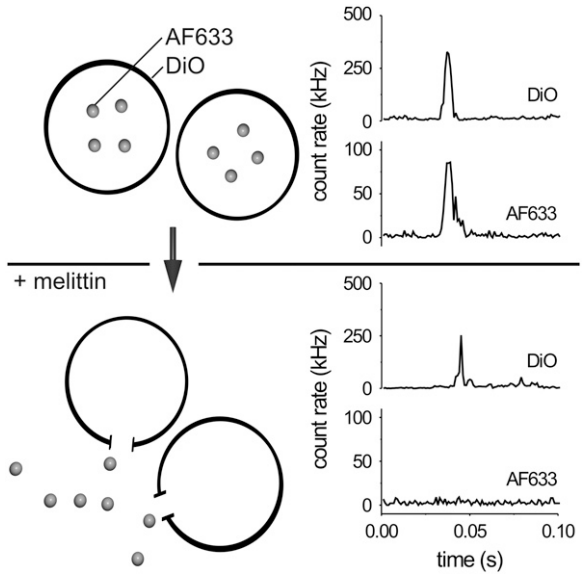

FIGURE 1 Principle of dual-color fluorescence-burst analysis. Liposomes labeled with the fluorescent lipid analog DiO and with encapsulated Alexa fluor 633 (AF633)-labeled size-marker molecules are depicted schematically. The fluorescent bursts, resulting from the diffusion of liposomes through the detection volume of a dual-color confocal microscope, are recorded for >10 min. Because both DiO and Alexa fluor 633 are liposome associated, the intensity bursts in both channels coincide. Addition of melittin results in pore formation and pore-size dependent leakage of the size-marker molecules from the liposomes and thereby, in turn, cancels out the coincidence of the fluorescence bursts.

typical intensity trace for liposomes consisting of 100% DOPC with encapsulated fluorescently labeled glutathione is shown. After addition of melittin, glutathione leaked out of the liposomes and the fluorescence bursts no longer coincided (Fig. 2 *B*). The same phenomenon was observed for liposomes composed of the anionic lipid DOPG (Fig. 2 *C–D*). Each individual burst from the fluorescent lipid analogs corresponds to a liposome diffusing through the detection volume, and, for such a liposome, the concentration of size-marker was calculated (Eq. 1). Because traces were recorded for longer than 10 min, the concentration distributions of large populations (typically >1000 liposomes) were obtained. Steady-state levels of efflux were reached, since the concentration distributions were stable for >24 h (not shown).

Fig. 3 *A* presents the concentration distribution at different melittin concentrations of DiO-labeled liposomes composed of DOPC with encapsulated Alexa fluor 633-labeled glutathione (Eq. 1). Upon addition of melittin, pores were formed and the glutathione leaked out, resulting in lower internal concentrations. Liposomes composed of DOPG showed a similar behavior, albeit at higher melittin concentrations (Fig. 3 *B*). Surprisingly, the number of liposomes decreased with increasing melittin concentration (the surface of the histogram corresponds to the concentration of liposomes). For liposomes composed of a mixture of DOPC/DOPE, both the size-marker concentration and the total number of liposomes dropped already at low melittin/lipid ratios (Fig. 3 *C*). This decrease of the liposome concentration was due to liposome fusion or aggregation, since the average DiO burst intensities increased in parallel (Fig. 4 *A*). Moreover, bright fluorescent micrometer-size particles were observed in microscopic images, which were not visible before the addition of melittin (Fig. 4 *B*). The detergent Triton X-100 (used at 0.05% v/v) fully dissolved the liposomes and completely abolished the bursts of both the fluorescent lipid analogs and the size-marker molecules (not shown).

Lipid composition dependence

To quantify the melittin activity for different lipid compositions, the total number of liposomes was plotted as a function of the melittin concentration. Typical curves are shown in Fig. 5 (*solid square*) for liposomes consisting of 100% DOPC (*A*), 100% DOPG (*B*), and a 3:7 ratio of DOPC/DOPE (*C*). Also, the average concentration of encapsulated size marker was calculated (Eq. 2), and for Alexa fluor 633-labeled glutathione, these are also shown in Fig. 5 (*solid circle*). For DOPC, glutathione leakage was observed already at very low melittin concentrations, whereas membrane fusion was not observed below melittin/lipid ratios of 0.4 (Fig. 5 *A*; only data up to 0.08 are shown). For DOPG, glutathione leakage was observed at concentrations about 10 times higher than for DOPC (Fig. 5 *B*). Interestingly, liposome fusion or aggregation was observed in the same concentration range as the leakage of contents. Similar behavior was observed for liposomes consisting of a 3:7 ratio of DOPC/DOPE (Fig. 5 *C*), albeit at significantly lower melittin concentrations than for DOPG (notice the differences in the scales of the *x* axes of Fig. 5, *B–C*). To obtain $C_{L,1/2}$, defined as the concentration of melittin where half of the liposomes released their content, the size-marker concentration curve (Fig. 5, *solid circle*, *solid line*) was fitted with a normal cumulative distribution function:

$$C_{av} = \frac{1}{2}\left(1 - \mathrm{erf}\frac{C_M - C_{L,1/2}}{\sigma\sqrt{2}}\right), \quad (3)$$

where C_{av} is the average size-marker concentration of the liposomes normalized to the condition where no melittin was present, C_M is the melittin concentration, σ^2 is the variance, and erf indicates the error function. Similarly, the melittin $C_{F,1/2}$ concentrations at which half of the liposomes were fused or aggregated (Fig. 5, *solid square*, *dotted line*) were calculated using Eq. 3, with C_{av} corresponding to the normalized number of liposomes.

The $C_{F,1/2}$-values for fusion or aggregation were determined for a number of lipid compositions. DOPC fused at melittin/lipid ratios of 0.44 ± 0.04. Addition of 10% cholesterol reduced the melittin/lipid ratio needed for fusion or aggregation to 0.25 ± 0.07 (Fig. 6 *A*). Liposomes consisting of 1:1 and 3:7 ratios of DOPC/DOPE fused or

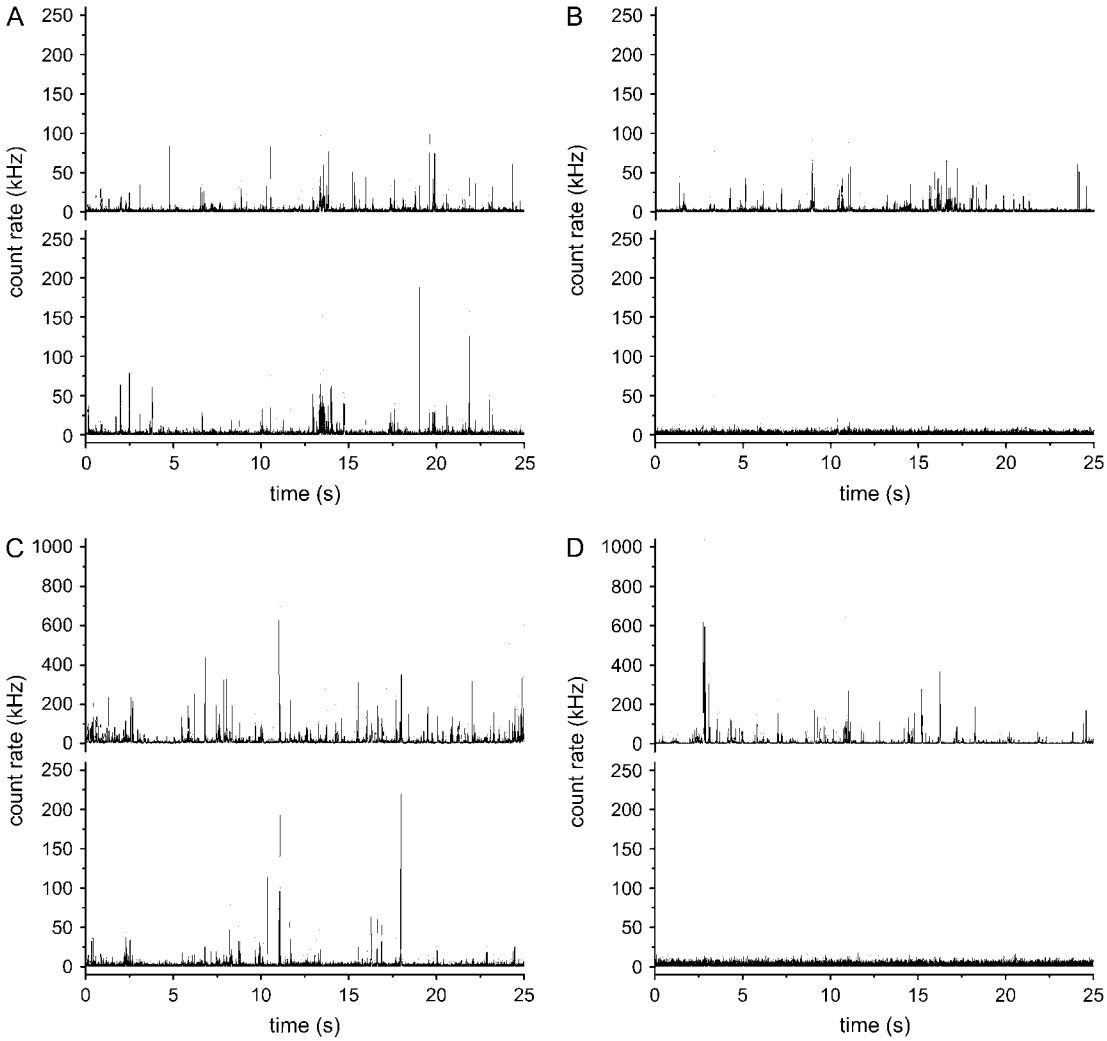

FIGURE 2 Fluorescence traces from DCFBA experiments. The upper panels show the intensity traces for the fluorescent lipid analog DiO and the lower panels the corresponding traces of the encapsulated Alexa fluor 633-labeled glutathione. Traces are shown for liposomes consisting of: DOPC without (*A*) and with melittin ((*B*) the melittin/lipid ratio was 0.03, which corresponds to a concentration of 4 μM), and DOPG without (*C*) and with melittin ((*D*) the melittin/lipid ratio was 0.09, which corresponds to a concentration of 12 μM). Melittin eliminates the bursts from Alexa fluor 633-labeled glutathione, because glutathione is no longer associated with the liposomes and the signal from individual molecules is low. Only the first 25 s of >10 min are shown.

aggregated at melittin/lipid ratios of 0.13 ± 0.03 and 0.004 ± 0.003, respectively. DOPE (100%) was not tested, since it did not form stable bilayers under the used experimental conditions (48). Similar to DOPE, DOPG decreased the amount of melittin needed to induce liposome fusion or aggregation, and, for 100% DOPG, this was induced at a melittin/lipid ratio of 0.06 ± 0.02. Analogous to liposome fusion or aggregation, the $C_{L,1/2}$-values were determined for leakage of different size markers (Fig. 6 *B*). Fluorescently labeled glutathione (1.4 kDa), BPTI (7.6 kDa), 10 kDa dextran (10 kDa), and α-lactalbumin (15.3 kDa) were used as size markers. In the case of 100% DOPC and DOPC with 10% cholesterol, the smaller size-marker molecules leaked out at lower melittin concentrations than the bigger ones, indicating a pore-size dependence on the melittin concentration. For liposomes containing synthetic DOPE or DOPG this size dependence was abolished (Fig. 6 *B*), suggesting that leakage is a consequence of the fusion or aggregation of the liposomes rather than formation of specific pores. The 70 kDa dextran was also tested for liposomes consisting of 100% DOPG or a 1:1 mixture of DOPC/DOPE, and this compound leaked out at similar melittin concentrations as the smaller size markers (not shown). Thus, in membranes with a fraction of DOPE or DOPG, melittin triggers the formation of holes with sizes of at least 2.3–5 nm (size of the largest size markers (45,46)). Interestingly, for liposomes consisting of *E. coli* total lipid extract, there was a melittin concentration dependence for the leakage of the three smallest size markers (Fig. 6 *B*), and hence a pore-size dependence. *E. coli* membranes consist of anionic lipids (phosphotidylglycerol (PG) plus cardiolipin) and phosphatidyletanolamine (PE) in a ratio of ~3:7 (49). The $C_{F,1/2}$-value for fusion or aggregation, but not the $C_{L,1/2}$-value for

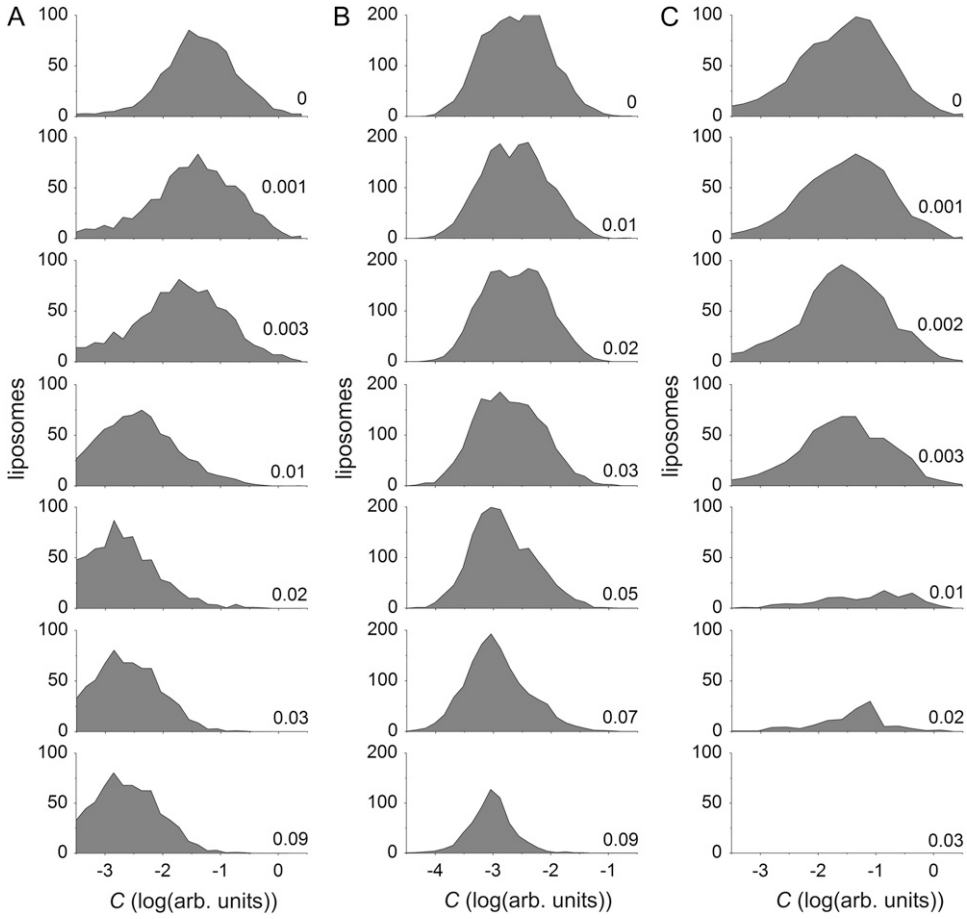

FIGURE 3 Pore formation of melittin. The distribution of Alexa fluor 633-labeled glutathione ((*C*) Eq. 1) over the liposomes is shown for various melittin/lipid ratios (ratios are indicated in the figure). The distributions are shown for liposomes consisting of: (*A*) DOPC, (*B*) DOPG, and (*C*) a 3:7 ratio of DOPC/DOPE. Upon the addition of melittin, the concentration of glutathione decreased due to leakage from the liposomes. Importantly, for DOPG and DOPC/DOPE the total number of liposomes (area of the histogram) also decreased upon the addition of melittin due to membrane fusion or aggregation. The bin width used was 0.16.

leakage, was similar for membranes consisting of a 3:7 mixture of DOPG/DOPE (0.03 ± 0.01, Fig. 6 *A*).

In vivo leakage experiments

DCFBA is based on the fluorescent labeling of liposomes and encapsulated size-marker molecules labeled with a second fluorophore. Here, we demonstrate that this approach can also be used to probe pore formation in bacteria instead of liposomes, using GFP as a leakage marker. *Lactococcus lactis* (strain MG1363) cells, expressing the OpuC-GFP fusion protein from a plasmid, were labeled with the red membrane probe DiD. OpuC is the 24 kDa substrate-binding domain of OpuA (an osmoregulated ABC transporter from *L. lactis*), expressed as a soluble protein (50). OpuC-GFP can be considered as two beads each with a Stokes radius of 2.8 nm (51). The inset of Fig. 7 shows confocal images of *L. lactis* cells expressing OpuC-GFP (*upper image*) and labeled

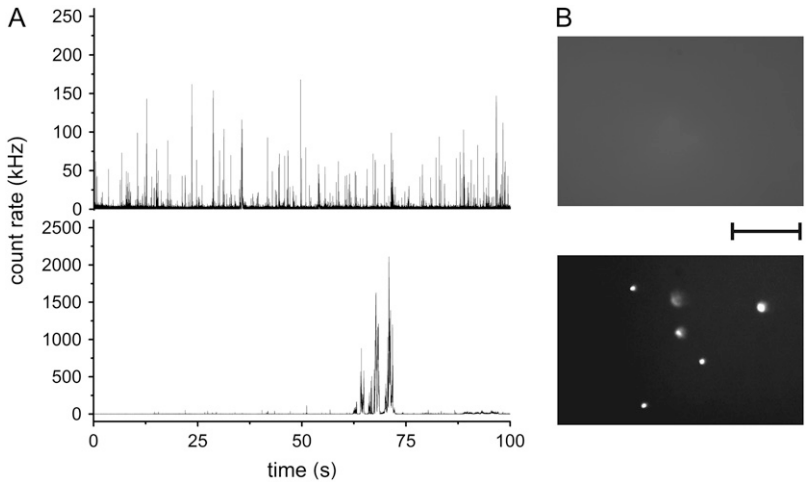

FIGURE 4 Melittin-induced fusion of liposomes consisting of 100% DOPG. (*A*) Fluorescence intensity traces of the fluorescent lipid analog DiO before (*upper graph*) and after the addition of a melittin (*lower graph*). Upon the addition of melittin (melittin/lipid ratio of 0.09; 12 μM), the number of fluorescence bursts (related to the liposome concentration) decreased and the average burst intensity increased. (*B*) Fluorescence microscopy images of the samples from panel *A*. After addition of melittin, micrometer-size particles became visible.

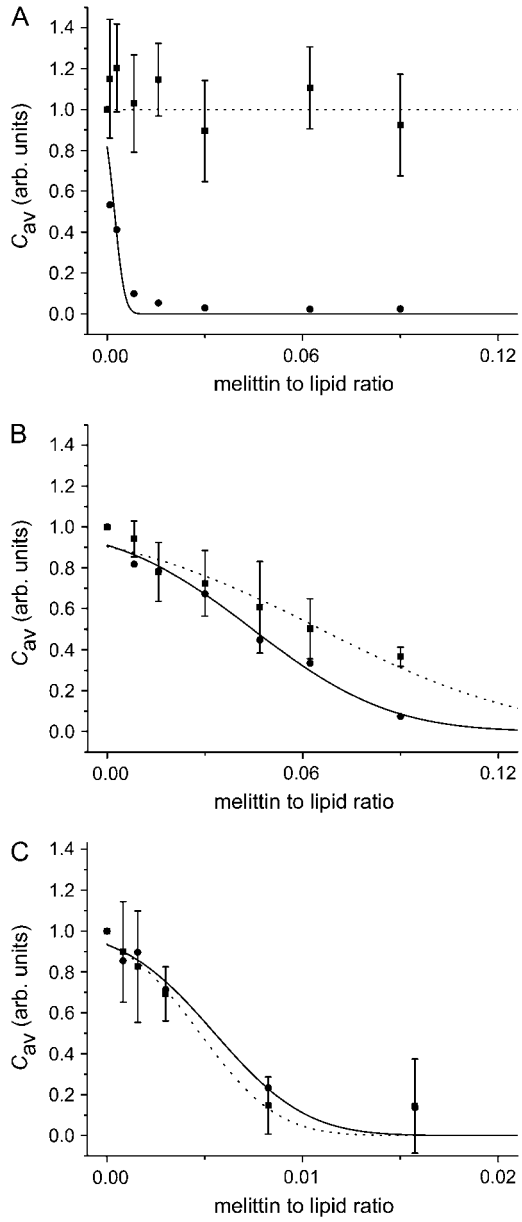

FIGURE 5 Melittin titration curves. Normalized, average glutathione concentrations (C_{av}, Eq. 2, ●) and total number of liposomes (■) plotted as a function of the melittin/lipid ratios for liposomes composed of: (*A*) DOPC, (*B*) DOPG, and (*C*) a 3:7 ratio of DOPC/DOPE. The data were normalized to the conditions where no melittin was present. For the total number of liposomes, the data sets for the four different size markers were averaged and the error bars show the standard deviation. The solid and dotted lines are fits with a cumulative distribution function (Eq. 3), used to obtain the melittin/lipid ratio where leakage or fusion was 50% ($C_{L,1/2}$- and $C_{F,1/2}$-values, respectively). For liposome fusion or aggregation, the $C_{F,1/2}$-values with spread σ^2 were as follows: (*A*) $C_{F,1/2} = 0.3$, $\sigma^2 = 0.9$ (40 μM), (*B*) $C_{F,1/2} = 0.07$, $\sigma^2 = 0.33$ (9.3 μM), and (*C*) $C_{F,1/2} = 0.005$, $\sigma^2 = 0.001$ (0.7 μM). For glutathione leakage, the $C_{L,1/2}$-values were: (*A*) $C_{L,1/2} = 0.002$, $\sigma^2 = 0.001$ (0.3 μM), (*B*) $C_{L,1/2} = 0.05$, $\sigma^2 = 0.15$ (6.7 μM), and (*C*) $C_{L,1/2} = 0.005$, $\sigma^2 = 0.002$ (0.7 μM).

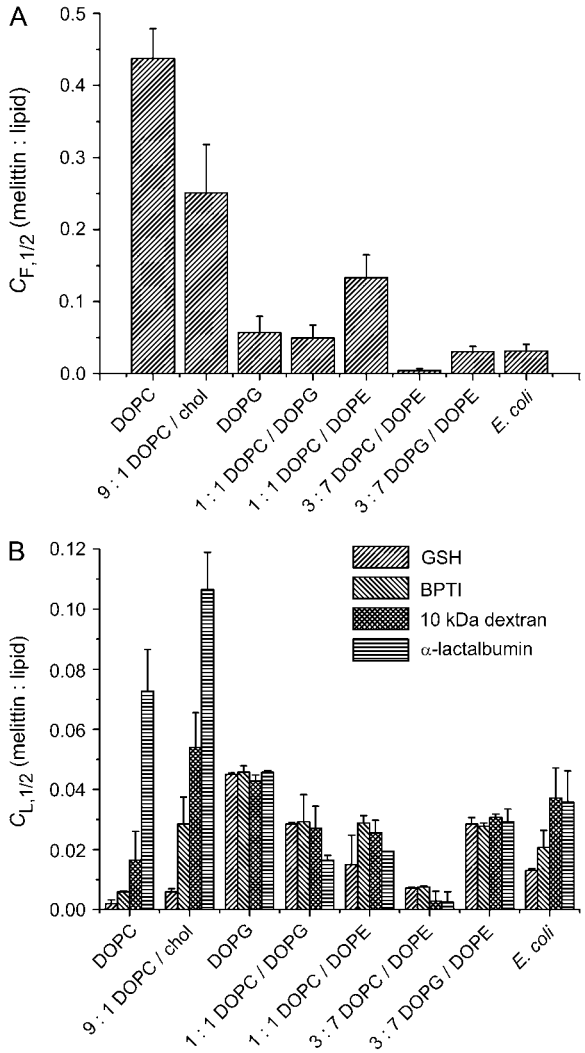

FIGURE 6 Melittin action on liposomes of various lipid compositions. (*A*) $C_{F,1/2}$-values for liposome fusion or aggregation, reflecting the melittin/lipid ratio where half of the liposomes were fused or aggregated. The bars represent the standard deviation for >10 measurements. (*B*) $C_{L,1/2}$-values for leakage of the fluorescent size-marker molecules. The size markers are arranged on increasing size: GSH, Alexa fluor 633-labeled glutathione (molecular mass, 1.4 kDa (45)); BPTI, Alexa fluor 633-labeled bovine pancreas tryptic inhibitor (7.6 kDa (45)); 10 kDa dextran, Alexa fluor 647-labeled dextran molecule (10 kDa); α-lactalbumin, Alexa fluor 633-labeled α-lactalbumin (15.3 kDa (45)).

with DiD (*lower image*). The main figure presents the GFP concentration before and after 5 min treatment with 4 μM melittin. As can be seen from the figure, melittin caused leakage of OpuC-GFP and thus formation of pores of at least 2.8 nm.

DISCUSSION

In the case of membranes prepared from 100% DOPC, Alexa fluor 633-labeled glutathione leaked out at melittin/lipid ratios of 0.002 ± 0.001, which is consistent with literature values for liposomes with PC headgroups and small

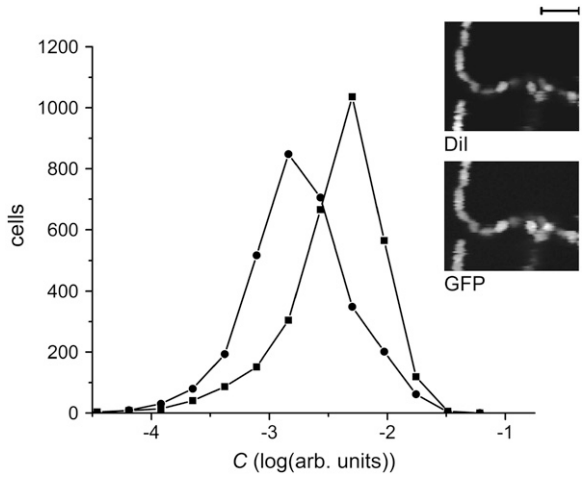

FIGURE 7 In vivo leakage experiment. DCFBA experiments were performed on *L. lactis* cells expressing a OpuC-GFP fusion protein of 51 kDa (*inset*, *bottom panel*). The cell membranes were stained with the red fluorescent lipid analog DiD (*inset*, *top panel*). The distribution of the GFP-fusion protein over the cells is presented in the main figure (■) After addition of 4 μM melittin, the GFP-fusion protein leaked from the cells and this resulted in a decrease of the internal GFP concentration (●).

size-marker molecules (20,34–36). Solid-state NMR studies have shown that melittin has a transmembrane orientation at these melittin/lipid ratios (22–24). For larger size-marker molecules, leakage occurred at higher melittin concentrations (Fig. 6 *B*), demonstrating that the pore size is related to the melittin concentration. It has been reported that at melittin/lipid ratios of <0.01, the fluorophore calcein leaked out, but not labeled dextran (Stokes radius of 1.3 and 2.4 nm, respectively), whereas at higher melittin concentrations both leaked out (36). Other studies also provide evidence for a certain relationship between the pore size and melittin concentration, since large size-marker molecules leaked to a lesser extent or at a higher melittin concentration than the smaller ones (34,35). At high melittin/lipid ratios of 0.44 ± 0.04, melittin fused or aggregated liposomes (Fig. 6 *A*). At this melittin/lipid ratio, the phospholipids structure is still that of a bilayer with minimal disruption (52,53). The fusogenic effect of melittin has been reported in the literature (35,54–56) but is now quantitatively differentiated from the formation of discrete pores. The presence of 10% cholesterol increased the melittin/lipid ratios needed for efflux, relative to 100% DOPC liposomes (Fig. 6 *B*), and the activity of melittin was reduced. It is well known that cholesterol reduces the pore-forming activity of melittin (5,9,26,43,57) and this is probably due to reduced binding of the peptide to the bilayer (58–60). The reduced melittin activity may also be accounted for by tight lipid packing and increased deformation energy induced by cholesterol (5).

Melittin was much less active in liposomes containing a fraction of DOPG than in liposomes of 100% DOPC liposomes (Fig. 6 *B*), whereas the absorption to the liposome surface of the cationic peptide is approximately sixfold higher (33). For 100% DOPG liposomes, melittin/lipid ratios of 0.045 ± 0.001 were needed to induce leakage of glutathione, and this is $\sim$25 times higher than that for 100% DOPC liposomes. For liposomes consisting of a 1:1 ratio of DOPC/DOPG, an intermediate melittin/lipid ratio of 0.028 ± 0.001 was needed to induce leakage (Fig. 6 *B*). It is well known that melittin is less active with negatively charged lipids like DOPG than with neutral lipids (26,35–42,61). This phenomenon has been explained by the difficulty in membranes with a negative surface charge to insert the melittin α-helix, which requires a reorientation of the molecule from parallel to perpendicular to the membrane plane. In membranes with negatively charged headgroups, the cationic melittin is more tightly bound in comparison to membranes with zwitterionic PC headgroups (4). This proposal is supported by the finding that PC membranes have a lower capacity for surface absorption of melittin in comparison to negatively charged bilayers (33).

Importantly, for DOPG-containing liposomes, there was no difference in melittin activity for the leakage of different size markers (Fig. 6 *B*). Thus, contrary to 100% DOPC liposomes, there was no relationship between the pore size and the melittin concentration and the holes formed must have been at least 3.2–5 nm in diameter (size of α-lactalbumin and 70 kDa dextran (45,46)). This is in agreement with the finding that PG-containing membranes have no preference for 4 and 70 kDa dextrans, whereas more of the smaller compound leaked out from zwitterionic PC membranes (4). Another important difference was that melittin induced fusion or aggregation of DOPG containing liposomes at similar concentrations as leakage, whereas for 100% DOPC liposomes, this concentration was 100–1000 times higher (Fig. 6). These findings are in accordance with turbidity measurements, where the size of small unilamellar vesicles increased for negative lipids, but not for neutral lipids (35,55). It has been suggested that melittin does not insert into PG-containing bilayers, but only accumulates at the surface and that this asymmetric accumulation eventually leads to nonselective membrane damage and efflux via nonspecific holes (4,58). This is supported by the finding that aggregation of surface-bound α-helical melittin leads to a reduced bilayer thickness (62–65) and consequently local structural instabilities and fluctuations (4). According to our findings, these nonselective pores coincide with fusion or aggregation (Fig. 5 *B*). Thus, in negatively charged membranes, melittin aggregates either in the membrane or on the membrane surface, which leads to fusion or aggregation of the lipid bilayers, accompanied by nonspecific contents leakage from the liposomes. These morphological changes of membranes induced by melittin occur only when the lipids are in the crystalline liquid phase and the hydrocarbon chains have a disordered conformation (32). It is well known that if the lipids are in the gel-phase, melittin induces micellization of the vesicles and, at high concentrations, a complete loss of vesicular structure via the carpet-like mechanism (31,32,37,57,66–69).

The presence of 50% DOPE had similar effects on the melittin activity as DOPG. Higher melittin concentrations were necessary to induce leakage of the smaller size-marker molecules from liposomes composed of a 1:1 mixture of DOPC/DOPE, compared to 100% DOPC. Also, all size-marker molecules leaked out at similar melittin concentrations and the pore-size dependency on the melittin concentration was lost (Fig. 6 *B*). DOPE is a nonbilayer forming lipid and promotes a negative membrane curvature (48). It is known that lipids of positive curvature (lysoPC) facilitate and lipids with negative curvature (PE) inhibit melittin pore formation (9,19,35). Lipids of positive curvature facilitate the bending of the membrane into the toroidal pore. Additionally, melittin binds with a 10–100-fold lower dissociation constant to membranes composed of PE/PG than to PC/PG (58,70), and this might prevent the pore formation. For liposomes consisting of a 1:1 ratio of DOPC/DOPE, fusion or aggregation occurred at melittin/lipid ratios of 0.13 ± 0.03 and this is approximately threefold lower than for 100% DOPC liposomes. This difference is probably due to the destabilizing effect of bilayers by PE (48), an effect that is opposed by melittin (53). A DOPE content of 70% resulted in liposome fusion or aggregation already at 0.004 ± 0.003 melittin/lipid ratio. The melittin concentrations needed for membrane fusion and contents leakage were much lower for liposomes consisting of a 3:7 ratio of DOPC/DOPE than for liposomes consisting of the same ratio of DOPG/DOPE (Fig. 6).

In conclusion, melittin has two different effects on membranes (Fig. 8): i), pore formation with the pore-size dependent on the melittin concentration; and ii), membrane fusion or aggregation accompanied by nonspecific leakage. The first effect was observed at low melittin concentrations for liposomes consisting of 100% DOPC or 90% DOPC with 10% cholesterol. The second effect dominated in all lipid mixtures containing the anionic lipid PG or the nonbilayer lipid PE. Interestingly, for liposomes consisting of *E. coli* total lipid extract, a melittin concentration dependence was observed for leakage of the three smallest size markers (Fig. 6 *B*). This was not observed for liposomes composed of a 3:7 ratio of DOPG/DOPE, which can be regarded as a mimic of the *E. coli* total lipid extract (49). This difference must be due to other factors, like acyl chain length, degree of fatty acid saturation, or the presence of tracer amounts of other lipids, which may cause a different lipid packing and hence binding of melittin. Whatever the basis for the difference is, our measurements emphasize the importance of comparing synthetic and native-like lipid mixtures in studying the pore formation of antimicrobial peptides. For another group of antimicrobial peptides (rabbit defensins), similar differences between *E. coli* and synthetic lipids have been reported (38,71). It was recently shown that melittin leads to aggregation of intact *Candida albicans*, *E. coli*, and *Staphylococcus aureus* cells (35), and probably both the pore formation and the leaky-fusion mechanism are relevant in vivo. DCFBA can be used for an in vivo leakage assay, as was shown in preliminary experiments with *L. lactis* cells expressing a GFP-fusion protein (Fig. 7).

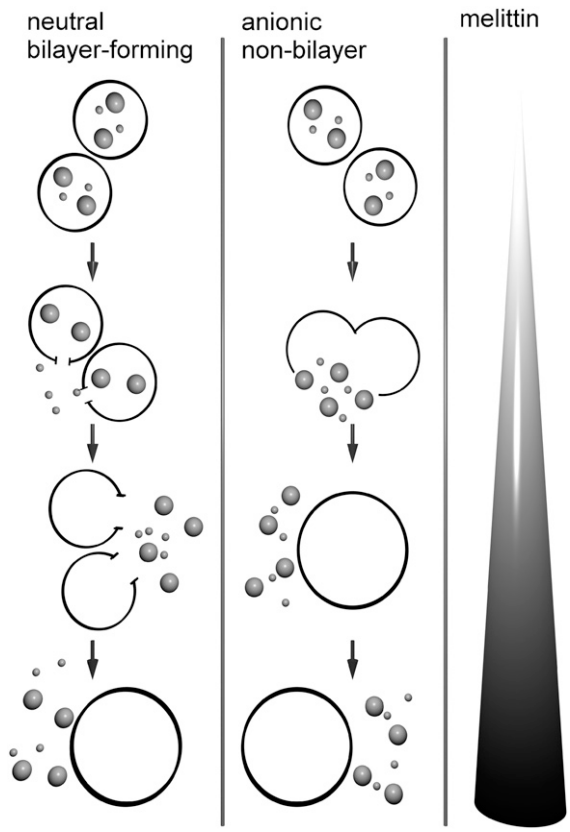

FIGURE 8 Model for the action of melittin. In membranes composed of neutral (zwitterionic), bilayer-forming lipids, low melittin concentrations induce pore formation. The pore size is dependent on the melittin concentration. A further increase in the melittin concentration will ultimately lead to membrane fusion or aggregation. In membranes containing anionic and/or nonbilayer forming lipids, melittin addition results in nonspecific membrane leakage and fusion or aggregation.

General techniques that have been employed to study antimicrobial peptides are x-ray crystallography, and optical, fluorescence, NMR, Fourier transform infrared, Raman, and circular dichroism spectroscopy (1). DCFBA is a powerful addition to these techniques, since it allows the detection of concentration distributions and is able to discriminate leakage from membrane fusion and lysis ((45); this work). It has further advantages of being relatively fast with acquisition times of ~10 min and using very little ($\sim\mu$g) material. Therefore, DCFBA enables medium-throughput screening of lipid compositions and size-marker molecules, and we intend to use it to study different antimicrobial peptides. One could also employ DCFBA to determine effects salt and osmotic gradients on melittin action and thereby obtain a better understanding of the in vivo effects (5,43).

We thank R.K.R. Marreddy and E.R. Geertsma for the kind gift of the plasmid for the OpuC-GFP construct.

We are grateful to the Dutch Science Foundation (NWO), grant number ALW-814.02.002, and the Zernike Institute for Advanced Materials for financial support.

REFERENCES

1. Brogden, K. A. 2005. Antimicrobial peptides: pore formers or metabolic inhibitors in bacteria? *Nat. Rev. Microbiol.* 3:238–250.
2. Finlay, B. B., and R. E. Hancock. 2004. Can innate immunity be enhanced to treat microbial infections? *Nat. Rev. Microbiol.* 2:497–504.
3. Hancock, R. E., and A. Patrzykat. 2002. Clinical development of cationic antimicrobial peptides: from natural to novel antibiotics. *Curr. Drug Targets Infect. Disord.* 2:79–83.
4. Ladokhin, A. S., and S. H. White. 2001. ''Detergent-like'' permeabilization of anionic lipid vesicles by melittin. *Biochim. Biophys. Acta.* 1514:253–260.
5. Raghuraman, H., and A. Chattopadhyay. 2007. Melittin: a membrane active peptide with diverse functions. *Biosci. Rep.* In press.
6. Habermann, E. 1972. Bee and wasp venom: the biochemistry and pharmacology of their peptides and enzymes are reviewed. *Science.* 177: 314–322.
7. Lauterwein, J., L. R. Brown, and K. Wuthrich. 1980. High-resolution 1H-NMR studies of monomeric melittin in aqueous solution. *Biochim. Biophys. Acta.* 622:219–230.
8. Talbot, J. C., J. Dufourcq, J. de Bony, J. F. Faucon, and C. Lussan. 1979. Conformational change and self association of monomeric melittin. *FEBS Lett.* 102:191–193.
9. Allende, D., S. A. Simon, and T. J. McIntosh. 2005. Melittin-induced bilayer leakage depends on lipid material properties: evidence for toroidal pores. *Biophys. J.* 88:1828–1837.
10. Iwadate, M., T. Asakura, and M. P. Williamson. 1998. The structure of the melittin tetramer at different temperatures—an NOE-based calculation with chemical shift refinement. *Eur. J. Biochem.* 257:479–487.
11. Inagaki, F., I. Shimada, K. Kawaguchi, M. Hirano, I. Terasawa, T. Ikura, and N. Go. 1989. Structure of melittin bound to perdeuterated dodecylphosphocholine micelles as studied by two-dimensional NMR and distance geometry calculations. *Biochemistry.* 28:5985–5991.
12. Ikura, T., N. Go, and F. Inagaki. 1991. Refined structure of melittin bound to perdeuterated dodecylphosphocholine micelles as studied by 2D-NMR and distance geometry calculation. *Proteins.* 9:81–89.
13. Vogel, H., and F. Jahnig. 1986. The structure of melittin in membranes. *Biophys. J.* 50:573–582.
14. Toke, O. 2005. Antimicrobial peptides: new candidates in the fight against bacterial infections. *Biopolymers.* 80:717–735.
15. Saini, S. S., A. K. Chopra, and J. W. Peterson. 1999. Melittin activates endogenous phospholipase D during cytolysis of human monocytic leukemia cells. *Toxicon.* 37:1605–1619.
16. Saini, S. S., A. K. Chopra, and J. W. Peterson. 2000. Melittin-mediated release of [3H]-oleic acid from *E. coli* cells is dependent upon heat- and trypsin-sensitive factor(s) in human serum. *Toxicon.* 38:1077–1086.
17. Oren, Z., and Y. Shai. 1997. Selective lysis of bacteria but not mammalian cells by diastereomers of melittin: structure-function study. *Biochemistry.* 36:1826–1835.
18. Shai, Y., and Z. Oren. 1996. Diastereoisomers of cytolysins, a novel class of potent antibacterial peptides. *J. Biol. Chem.* 271: 7305–7308.
19. Lee, M. T., F. Y. Chen, and H. W. Huang. 2004. Energetics of pore formation induced by membrane active peptides. *Biochemistry.* 43: 3590–3599.
20. Yang, L., T. A. Harroun, T. M. Weiss, L. Ding, and H. W. Huang. 2001. Barrel-stave model or toroidal model? A case study on melittin pores. *Biophys. J.* 81:1475–1485.
21. Sansom, M. P. 1991. The biophysics of peptide models of ion channels. *Prog. Biophys. Mol. Biol.* 55:139–215.
22. Naito, A., T. Nagao, K. Norisada, T. Mizuno, S. Tuzi, and H. Saito. 2000. Conformation and dynamics of melittin bound to magnetically oriented lipid bilayers by solid-state (31)P and (13)C NMR spectroscopy. *Biophys. J.* 78:2405–2417.
23. Smith, R., F. Separovic, T. J. Milne, A. Whittaker, F. M. Bennett, B. A. Cornell, and A. Makriyannis. 1994. Structure and orientation of the pore-forming peptide, melittin, in lipid bilayers. *J. Mol. Biol.* 241:456–466.
24. Lam, Y.-H., S. R. Wassall, C. J. Morton, R. Smith, and F. Separovic. 2001. Solid-State NMR structure determination of melittin in a lipid environment. *Biophys. J.* 81:2752–2761.
25. Ludtke, S. J., K. He, W. T. Heller, T. A. Harroun, L. Yang, and H. W. Huang. 1996. Membrane pores induced by magainin. *Biochemistry.* 35: 13723–13728.
26. Gómara, M. J., S. Nir, and J. L. Nieva. 2003. Effects of sphingomyelin on melittin pore formation. *Biochim. Biophys. Acta.* 1612:83–99.
27. Hristova, K., C. E. Dempsey, and S. H. White. 2001. Structure, location, and lipid perturbations of melittin at the membrane interface. *Biophys. J.* 80:801–811.
28. Citra, M. J., and P. H. Axelsen. 1996. Determination of molecular order in supported lipid membranes by internal reflection Fourier transform infrared spectroscopy. *Biophys. J.* 71:1796–1805.
29. Altenbach, C., W. Froncisz, J. S. Hyde, and W. L. Hubbell. 1989. Conformation of spin-labeled melittin at membrane surfaces investigated by pulse saturation recovery and continuous wave power saturation electron paramagnetic resonance. *Biophys. J.* 56:1183–1191.
30. Stanislawski, B., and H. Rterjans. 1987. 13C-NMR investigation of the insertion of the bee venom melittin into lecithin vesicles. *Eur. Biophys. J.* 15:1–15.
31. Dempsey, C. E., and G. S. Butler. 1992. Helical structure and orientation of melittin in dispersed phospholipid membranes from amide exchange analysis *in situ*. *Biochemistry.* 31:11973–11977.
32. Dufourcq, J., J. F. Faucon, G. Fourche, J. L. Dasseux, M. le Maire, and T. Gulik-Krzywicki. 1986. Morphological changes of phosphatidylcholine bilayers induced by melittin: vesicularization, fusion, discoidal particles. *Biochim. Biophys. Acta.* 859:33–48.
33. Kleinschmidt, J. H., J. E. Mahaney, D. D. Thomas, and D. Marsh. 1997. Interaction of bee venom melittin with zwitterionic and negatively charged phospholipid bilayers: a spin-label electron spin resonance study. *Biophys. J.* 72:767–778.
34. Ladokhin, A. S., M. E. Selsted, and S. H. White. 1997. Sizing membrane pores in lipid vesicles by leakage of co-encapsulated markers: pore formation by melittin. *Biophys. J.* 72:1762–1766.
35. Park, S. C., J. Y. Kim, S. O. Shin, C. Y. Jeong, M. H. Kim, S. Y. Shin, G. W. Cheong, Y. Park, and K. S. Hahm. 2006. Investigation of toroidal pore and oligomerization by melittin using transmission electron microscopy. *Biochem. Biophys. Res. Commun.* 343:222–228.
36. Matsuzaki, K., S. Yoneyama, and K. Miyajima. 1997. Pore formation and translocation of melittin. *Biophys. J.* 73:831–838.
37. Matsuzaki, K., O. Murase, and K. Miyajima. 1995. Kinetics of pore formation by an antimicrobial peptide, magainin 2, in phospholipid bilayers. *Biochemistry.* 34:12553–12559.
38. Hristova, K., M. E. Selsted, and S. H. White. 1997. Critical role of lipid composition in membrane permeabilization by rabbit neutrophil defensins. *J. Biol. Chem.* 272:24224–24233.
39. Kang, J. H., S. Y. Shin, S. Y. Jang, M. K. Lee, and K. S. Hahm. 1998. Release of aqueous contents from phospholipid vesicles induced by cecropin A (1–8)-magainin 2 (1–12) hybrid and its analogues. *J. Pept. Res.* 52:45–50.
40. Zhao, H., J. P. Mattila, J. M. Holopainen, and P. K. Kinnunen. 2001. Comparison of the membrane association of two antimicrobial peptides, magainin 2 and indolicidin. *Biophys. J.* 81:2979–2991.
41. Ambroggio, E. E., F. Separovic, J. H. Bowie, G. D. Fidelio, and L. A. Bagatolli. 2005. Direct visualization of membrane leakage induced by the antibiotic peptides: maculatin, citropin, and aurein. *Biophys. J.* 89:1874–1881.

42. Benachir, T., and M. Lafleur. 1995. Study of vesicle leakage induced by melittin. *Biochim. Biophys. Acta.* 1235:452–460.

43. Benachir, T., and M. Lafleur. 1996. Osmotic and pH transmembrane gradients control the lytic power of melittin. *Biophys. J.* 70:831–840.

44. Katsu, T., C. Ninomiya, M. Kuroko, H. Kobayashi, T. Hirota, and Y. Fujita. 1988. Action mechanism of amphipathic peptides gramicidin S and melittin on erythrocyte membrane. *Biochim. Biophys. Acta.* 939:57–63.

45. Van den Bogaart, G., V. Krasnikov, and B. Poolman. 2007. Dual-color fluorescence-burst analysis to probe protein efflux through the mechanosensitive channel MscL. *Biophys. J.* 92:1233–1240.

46. Laurent, T. C., and K. A. Granath. 1967. Fractionation of dextran and Ficoll by chromatography on Sephadex G-200. *Biochim. Biophys. Acta.* 136:191–198.

47. Bohrer, M. P., W. M. Deen, C. R. Robertson, J. L. Troy, and B. M. Brenner. 1979. Influence of molecular configuration on the passage of macromolecules across the glomerular capillary wall. *J. Gen. Physiol.* 74:583–593.

48. Hui, S. W., T. P. Stewart, P. L. Yeagle, and A. D. Albert. 1981. Bilayer to non-bilayer transition in mixtures of phosphatidylethanolamine and phosphatidylcholine: implications for membrane properties. *Arch. Biochem. Biophys.* 207:227–240.

49. Goodsell, D. S. 1991. Inside a living cell. *Trends Biochem. Sci.* 16: 203–206.

50. Biemans-Oldehinkel, E., and B. Poolman. 2003. On the role of the two extracytoplasmic substrate-binding domains in the ABC transporter OpuA. *EMBO J.* 22:5983–5993.

51. Terry, B. R., E. K. Matthews, and J. Haseloff. 1995. Molecular characterisation of recombinant green fluorescent protein by fluorescence correlation microscopy. *Biochem. Biophys. Res. Commun.* 217:21–27.

52. Smith, R., F. Separovic, F. C. Bennett, and B. A. Cornell. 1992. Melittin-induced changes in lipid multilayers. A solid-state NMR study. *Biophys. J.* 63:469–474.

53. Batenburg, A. M., J. H. van Esch, and B. de Kruijff. 1988. Melittin-induced changes of the macroscopic structure of phosphatidylethanolamines. *Biochemistry.* 27:2324–2331.

54. Morgan, C. G., H. Williamson, S. Fuller, and B. Hudson. 1983. Melittin induces fusion of unilamellar phospholipid vesicles. *Biochim. Biophys. Acta.* 732:668–674.

55. Higashino, Y., A. Matsui, and K. Ohki. 2001. Membrane fusion between liposomes composed of acidic phospholipids and neutral phospholipids induced by melittin: a differential scanning calorimetric study. *J. Biochem.* (*Tokyo*). 130:393–397.

56. Eytan, G. D., and T. Almary. 1983. Melittin-induced fusion of acidic liposomes. *FEBS Lett.* 156:29–32.

57. Monette, M., M. R. van Calsteren, and M. Lafleur. 1993. Effect of cholesterol on the polymorphism of dipalmitoylphosphatidylcholine/melittin complexes: an NMR study. *Biochim. Biophys. Acta.* 1149: 319–328.

58. Papo, N., and Y. Shai. 2003. Exploring peptide membrane interaction using surface plasmon resonance: differentiation between pore formation versus membrane disruption by lytic peptides. *Biochemistry.* 42:458–466.

59. Benachir, T., M. Monette, J. Grenier, and M. Lafleur. 1997. Melittin-induced leakage from phosphatidylcholine vesicles is modulated by cholesterol: a property used for membrane targeting. *Eur. Biophys. J.* 25:201–210.

60. Raghuraman, H., and A. Chattopadhyay. 2004. Interaction of melittin with membrane cholesterol: a fluorescence approach. *Biophys. J.* 87: 2419–2432.

61. Hincha, D. K., and J. H. Crowe. 1996. The lytic activity of the bee venom peptide melittin is strongly reduced by the presence of negatively charged phospholipids or chloroplast galactolipids in the membranes of phosphatidylcholine large unilamellar vesicles. *Biochim. Biophys. Acta.* 1284:162–170.

62. Huang, H. W. 2006. Molecular mechanism of antimicrobial peptides: the origin of cooperativity. *Biochim. Biophys. Acta.* 1758: 1292–1302.

63. Hristova, K., W. C. Wimley, V. K. Mishra, G. M. Anantharamiah, J. P. Segrest, and S. H. White. 1999. An amphipathic alpha-helix at a membrane interface: a structural study using a novel X-ray diffraction method. *J. Mol. Biol.* 290:99–117.

64. Wu, Y., K. He, S. J. Ludtke, and H. W. Huang. 1995. X-ray diffraction study of lipid bilayer membranes interacting with amphiphilic helical peptides: diphytanoyl phosphatidylcholine with alamethicin at low concentrations. *Biophys. J.* 68:2361–2369.

65. Jacobs, R. E., and S. H. White. 1989. The nature of the hydrophobic binding of small peptides at the bilayer interface: implications for the insertion of transbilayer helices. *Biochemistry.* 28:3421–3437.

66. Dufourcq, J., B. Clin, and B. Lemanceau. 1972. NMR study of ganglion-blocking and curare-like dimethoniums conformation in aqueous solutions. *FEBS Lett.* 22:205–209.

67. Dufourc, E. J., I. C. Smith, and J. Dufourcq. 1986. Molecular details of melittin-induced lysis of phospholipid membranes as revealed by deuterium and phosphorus NMR. *Biochemistry.* 25:6448–6455.

68. Monette, M., and M. Lafleur. 1996. Influence of lipid chain unsaturation on melittin-induced micellization. *Biophys. J.* 70:2195–2202.

69. Pott, T., M. Paternostre, and E. J. Dufourc. 1998. A comparative study of the action of melittin on sphingomyelin and phosphatidylcholine bilayers. *Eur. Biophys. J.* 27:237–245.

70. Carmieli, R., N. Papo, H. Zimmermann, A. Potapov, Y. Shai, and D. Goldfarb. 2006. Utilizing ESEEM spectroscopy to locate the position of specific regions of membrane-active peptides within model membranes. *Biophys. J.* 90:492–505.

71. Hristova, K., M. E. Selsted, and S. H. White. 1996. Interactions of monomeric rabbit neutrophil defensins with bilayers: comparison with dimeric human defensin HNP-2. *Biochemistry.* 35:11888–11894.